International Journal of Mechanical, Industrial and Aerospace Sciences
ISSN: 2517-9950
Vol:8, No:12, 2014

Scaling Strategy of a New Experimental Rig for Wheel-Rail Contact

Meysam Naeimi, Zili Li, Rolf Dollevoet

***Abstract*—**A new small–scale test rig developed for rolling contact fatigue (RCF) investigations in wheel–rail material. This paper presents the scaling strategy of the rig based on dimensional analysis and mechanical modelling. The new experimental rig is indeed a spinning frame structure with multiple wheel components over a fixed rail-track ring, capable of simulating continuous wheel-rail contact in a laboratory scale. This paper describes the dimensional design of the rig, to derive its overall scaling strategy and to determine the key elements' specifications. Finite element (FE) modelling is used to simulate the mechanical behavior of the rig with two sample scale factors of 1/5 and 1/7. The results of FE models are compared with the actual railway system to observe the effectiveness of the chosen scales. The mechanical properties of the components and variables of the system are finally determined through the design process.

***Keywords*—**New test rig, rolling contact fatigue, rail, small scale.

I. Introduction

INCREASING the rail lifetime by optimizing the steel microstructure and mechanical design is becoming more important as the railways increasingly claim for higher speeds, train frequencies and larger loading capacities. Improvement in rail material results in mitigating maintenance costs and preventing the rail degradation caused by rolling contact fatigue (RCF), which is occurred by the repeated rolling contact of wheels on rails. According to [1], [2] the highest stress levels occur at the running surface of the rail, where the wheel–rail contact stresses typically can reach 1500 MP for an axle load of 25 tones. Therefore, various sorts of RCF damages can be initiated and grown in rail material.

There is a large volume of published studies by taking the mechanical aspect of RCF into account, describing the importance of dynamic loading condition on rail fracture mechanics. Some examples of early works on this can be found in [3]-[6] while [7]-[10] are several examples of recent investigations on RCF and rail fracture mechanics using numerical approaches. Considering the microstructural and metallurgical prospective as the subject of research on RCF, a considerable amount of literature can be found too. Some of the most extensive research works of rail metallurgical investigations for instance are addressed in [11]-[15]. To optimize rail steel, a fundamental insight on the relations between mechanical loading, damage development and microstructural features is required. This allows fully understand the performance of different rail grades under wheel rail contact forces. In order to study the effect of rail material changing on FCF initiation by taking both mechanical and microstructural aspects into account, a new small-scale test rig is developed. The new test facility is a reduced scale rig consisting of several wheel components each of them rotates around a central pivot over a ring–shape rail track bed. A schematic view of the rig is shown in Fig. 1. The wheel assembly, composing of several subassemblies representative for the railway vehicle, is supported by a flat frame system above the track ring. The rail track assembly is composed of different subassemblies as the components of railway track structure, which is bended around a central pivot to provide a circular rail ring. The surface of the rail profile is the provided running band in contact with the wheel tread.

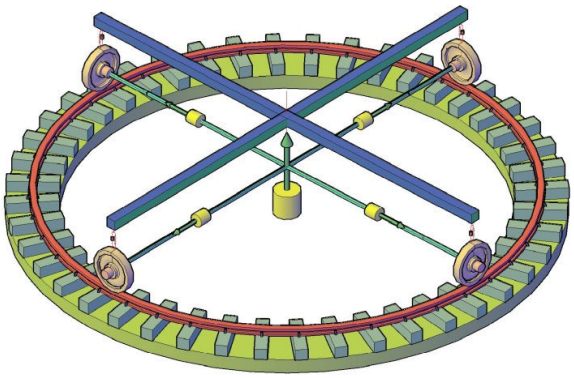

Fig. 1 Schematic view of the new test rig (multiple wheel on single rail track)

The initial stage in design process of the new rig involves dimensional analysis and determination of a proper scale strategy for the test facility. The scaling strategy is one of the most important aspects of the rig's design as it ensures that the selected parameters are correctly related and obey laws of similarity [16]. Finite element (FE) modelling is adopted to simulate the operational concept of the test rig and determine its mechanical performance. The design is evolved from the rig concept, in which a continuous wheel–rail contact happens. The present paper deals in particular with the dimensional evaluation and structural aspects of the new rig to determine the specifications and parameters of the system.

Meysam Naeimi, Zili Li and Rolf Dollevoet are with the Section of Railway Engineering, Faculty of Civil Engineering and Geoscience, Delft University of Technology, Stevin II Lab, Stevinweg 1, 2628 CN Delft, the Netherlands (e-mail: m.naeimi@tudelft.nl).

II. Scaling Strategy

A. Scaling Law

There are various approaches available to scaling. Early workers used the methods of dimensional analysis to establish several dimensionless groups, in which the scaling factors could be derived for each parameter [17], [18]. Others first derive the equations of motion and then calculate scaling factors required for each term to maintain the similarity [18]. Choice of material properties is also an important factor in the scaling method, and in addition influences the loading conditions required for similarity. The starting point for the following considerations to define similarity of railway system, is the geometric scaling, i.e. the definition of the scaling factor for all dimensions in the new test rig. General scaling rules can be used to relate the scale rig to its full size equivalent. References [16]-[23] are some examples of studies on scaling in railway. Most of these approaches are based on reducing all dimensions by the scale factor N, whereas the material properties are kept the same. Thus, a model structure is obtained with natural frequencies that are multiplied by the factor N [22]. As discussed in [16], a scaling strategy need to be selected based on the type of analysis work to be carried out in the test rig. The application of wheel–track rig in this research, allows railway track parameters to be evaluated in the tests. Therefore actual material properties have been considered without the application of scaling of material specifications. This allows almost an exact treatment of the wheel-rail material in contact conditions. As the rig in the current research is going to be extensively used for contact mechanics studies, the scaling strategy of [17], [22], [23] seems to be a more sensible approach due to the common objectives. This scaling strategy reduces all dimensions of the system with a linear scale factor, as well as the time parameter. The speed parameter therefore remains unchanged. Consider the identical material properties in the scaled test rig, other parameters and variables are obtained based on their relations to the time and distance. The main advantage for application of this scaling law is that the stress and strain parameters are remained unvaried in the test rig environment. The possible strategies of scaling are classified and comparatively evaluated in [16]. It should be realized that the scaled rig has different source of errors introduced by the scaling strategy, as a perfect scaling for all parameters cannot be achieved. This means that after determining the initial parameters of the system through dimensional analysis, additional calibrations will be needed from engineering viewpoints. Using the selected scaling strategy as a basis, the scaling factors given in Table I, are derived for parameters of the test rig. The value N in this table stands for the overall scale of the test rig, while the corresponding factors of different parameters are shown with ϕ values.

TABLE I
THE SCALE FACTORS FOR DIFFERENT PARAMETERS AND VARIABLES

Variable/ parameter	Variable notation	Units	Scale factor notation	Scale factor
Distance	L	m	ϕ_L	1/N
Cross section	A	m^2	ϕ_A	$1/N^2$
Volume	Vol.	m^3	ϕ_{Vol}	$1/N^3$
Second moment of area	I	m^4	ϕ_I	$1/N^4$
Density	ρ	kg/m3	ϕ_ρ	1
Mass	M	kg	ϕ_M	$1/N^3$
Young's modulus	E	N/m^2	ϕ_E	1
Poisson's ratio	ν	None	ϕ_ν	1
Mass per unit length	ρ.A	kg/m	$\phi_{\rho A}$	$1/N^2$
Force	F	N	ϕ_F	$1/N^2$
Creep/tangent forces	T	N	ϕ_T	$1/N^2$
Stress	σ	N/m^2	ϕ_σ	1
Strain	ε	None	ϕ_ε	1
Stiffness	K	N/m	ϕ_K	1/N
Damping	C	N.s/m	ϕ_C	$1/N^2$
Frequency	f	Hz	ϕ_f	N
Time	t	s	ϕ_t	1/N
Velocity	V	m/s	ϕ_V	1
Acceleration	a	m/s^2	ϕ_a	N
Friction coefficient	μ	None	ϕ_μ	1

As indicated in Table I, the value of each parameter is obtained by keeping the quantities of material specification unchanged (like density ρ, Young's modulus E, coefficient of friction μ etc.). The linear scale factor of 1/N is used for distance and time. The other parameters are determined based on their logical relationships with them. For instance, the scale factor for parameter M is obtained by keeping the density ρ constant, and simply deriving the scale factor of $1/N^3$ likewise to the volume, using the relevant equation: $M= \rho V$. Other parameters are calculated using the same procedure.

B. Selection of the Overall Scale

According to the scale factors in Table I, it is apparent that the overall scale of the rig (parameter N) has a significant influence over all variables. For the test rig of the current research two values of N=5 and N=7 are selected as the overall rig's scale and all corresponding variables are determined based on them. It is noteworthy that N is primarily defined as the ratio of the wheel diameter in the rig to that of actual railway vehicle. The reason for choosing these quantities of N is given subsequently:

1) The Scale of 1/7

According to the available history of the scaled test rigs in railway [16], [24], the least scale factor of the wheel is considered around 1/7, which stands for a disc seven times smaller than a real train wheel. Another implication of this (N=7) is possibly because the maximum diameter of a wheel disc that can be practically extracted from an actual wheel is approximately 130mm (N=920/130~7). This happens when the disc is extracted from the wheel's surrounding rim. This is because the maximum available width of an actual wheel is around 135mm (Fig. 2) and the wheel disc can be cut and machined from the wheel circumference (accumulated steel

part). Therefore, this value is the biggest radius of the wheel specimen that can be extracted from an original wheel.

2) The Scale of 1/5

It is intended to simulate the real contact mechanism of the wheel on track within the new test rig. As shown subsequently, the value of N=7 suggests a very small contact patch between wheel and rail. Small contact patch is not practically desirable for the emersion of RCF defects on rail as the size of defects may have relation to the patch size. Although N=7 offers the advantage of having a wheel specimen extracted from original wheel, it does not reflects small contact patch. Larger wheel up to 1/5 scale is therefore considered in the examinations as another choice. Of course, the wheel specimen with this size needs to be prepared from the gross steel bar. On the other hand, as the size of wheel increases, the overall scale of the test facility rises up. The smaller test rig benefits from lower weights, fewer costs of establishment, more convenience to conduct the tests and better monitoring and controlling conditions. Therefore, the maximum scale of N=5 is chosen by some try and error calculations as the upper limit for the new test rig. The wheel discs larger than 1/5 and smaller than 1/7 are therefore avoided.

C. Scaled Values of Parameters

Applying the prescribed values of N, the results of dimensional analysis for the equivalent one–fifth and one–seventh scaled rigs are determined as shown in Tables II and III. The values of actual vehicle–track system were obtained from [25] for the wheel profile S1002, rail profile UIC54E1 and typical concrete sleepers, fasteners and ballast in the Netherlands. Corresponding values of parameters for the scaled cases are calculated using the proposed scale factors of Table I.

TABLE II
MECHANICAL PARAMETERS OF ACTUAL SYSTEM AND THE TEST RIG

Mechanical variables (unit)	Actual	1/5 rig	1/7 rig
Lumped sprung mass, M_c (kg)	12000	480	245
Wheel weight (kg)	900	7.20	2.62
Rail weight per length (Kg/m)	54.42	2.18	1.11
Sleeper mass M_s (kg)	200	1.60	0.58
Friction coefficient	0.3	0.3	0.3
Traction coefficient	0.15	0.15	0.15
Average rolling speed (km/h)	60	60	60
Young's modulus of wheel–rail material, E_r (GP)	210	210	210
Poisson's ratio of wheel–rail, ν_r	0.3	0.3	0.3
Density of rail, ρ_r (kg/m3)	7800	7800	7800
Yield stress–hardened rail (GP)	1.12	1.12	1.12
Young's modulus of concrete material, E_c (GP)	38	38	38
Poisson's ratio of sleeper, ν_c	0.2	0.2	0.2
Density of sleeper, ρ_c (kg/m3)	2500	2500	2500

D. Geometric Design of the Rig by Two Scales

The chosen values of N are applied on the wheel–track components to extract the scaled geometry of the rig's components. The precise target values of the geometric parameters in the full–scale condition are demonstrated in Fig. 2. Based on a linear scaling method, the corresponding geometry of one–fifth and one–seventh scaled equivalents, are presented in Fig. 3. The geometries of wheel, rail and sleeper components are demonstrated in the figure.

TABLE III
GEOMETRICAL PARAMETERS OF ACTUAL SYSTEM AND THE TEST RIG

Mechanical variables (unit)	Actual	1/5 rig	1/7 rig
Rail Area, A_r (mm^2)	6977.00	279.08	142.39
Railhead lateral radius (mm)	300	60.00	42.86
Rail height, H_r (mm)	159.00	31.80	22.71
Rail head width (mm)	70.00	14.00	10.00
Rail head height (mm)	49.40	9.88	7.06
Rail inclination angle	1:40	1:40	1:40
Wheel radius, ϕ (mm)	460	92.00	65.71
Wheel width at centre (mm)	170	34.00	24.29
Wheel width at tread (mm)	135	27.00	19.29
Wheel web thickness (mm)	22	4.40	3.14
Wheel rim thickness (mm)	50	10.00	7.14
Wheel axle diameter (mm)	186	37.20	26.57
Sleeper spacing (mm)	600	120.00	85.71
Sleeper in half-track (mm)	1020	204.00	145.71
Sleeper width (mm)	250	50.00	35.71
Sleeper depth (mm)	220	44.00	31.43
Half–track width (mm)	1020	204.00	145.71
Ballast depth under sleeper	300	60.00	42.86
Rail pad dimensions (mm)	150*200	30*40	25*30

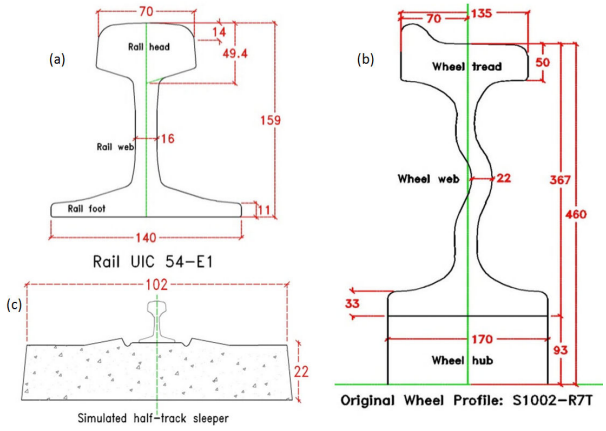

Fig. 2 Actual /full–size components, rail (a), wheel (b), sleeper (c), for normal Dutch railway, all dimensions are in mm

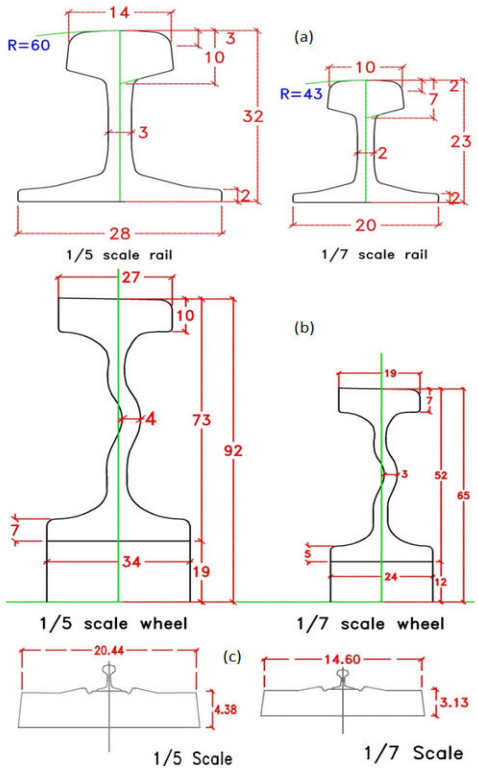

Fig. 3 Geometry of components in 1/5 and 1/7 scaled test rigs, all dimensions are in mm, (a) rails, (b) wheels, (c) sleepers

Fig. 4 demonstrates the cross section of wheel– rail track system based on the proposed geometries of the scaled test rigs. As described, the rail is mounted on discrete support elements, equivalent to the actual railway.

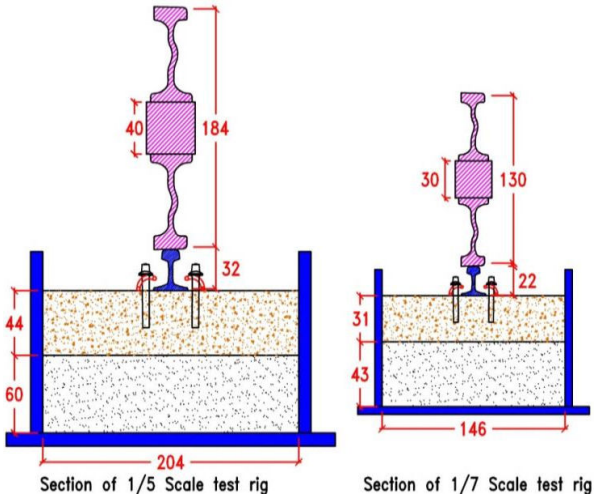

Fig. 4 Cross section of the wheel–track system in 1/5 and 1/7 test rigs

III. Mechanical Modelling of the Test Rig

So far, the overall scaling strategy of the new test rig is described. This section aims at finite element (FE) modelling of the scaled rig to predict its mechanical performance with respect to the wheel–rail contact mechanics. The schematic diagram of the vehicle–track FE model is shown in Fig. 5. Apart from the actual size model (Fig. 2), the wheel and rail profiles are obtained by scaling the actual geometries down to the order of five and seven (see the geometries in Fig. 3). Therefore, three FE models are built, one for the actual railway case, and two for the 1/5 scale and 1/7 scale test rigs. No flange is considered for wheel profile since the contact occurs in the lateral center of the rail top against the wheel tread. The sprung mass, which together with the unsprung mass (wheel weight) forms the wheel load, is lumped and supported by a group of springs and dampers of the primary suspension.

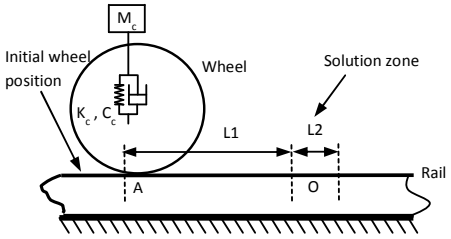

Fig. 5 The vehicle–track model in longitudinal –vertical direction

In contrast, the FE simulations aims to study the steady state contact mechanics of wheel–rail material with different scale strategies. To ensure that the results of the FE models are only due to the wheel–rail geometry change (not the dynamic characteristics), the vibration and wave propagation need to be minimized. This is achieved by supporting the rail material continuously on a rigid foundation (see Fig. 5), and by relaxing the dynamic process of the wheel–on–rail rolling until a steady state is achieved. In order to reduce the size of FE models, it is also possible to model only the upper part of the rail section (railhead) as it is rigidly fixed over the foundation. The FE models of the three discussed alternatives (actual case, 1/5 scale rig and 1/7 scale rig) are shown in Fig. 6.

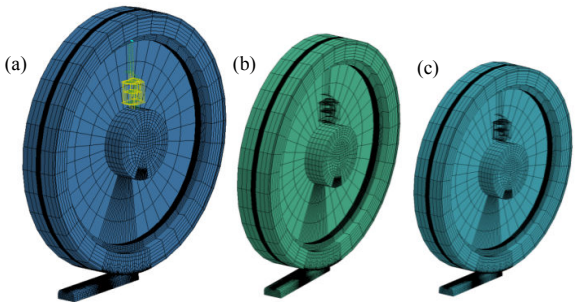

Fig. 6 The FE models of wheel–rail system for various scenarios, (a) Case-1, actual wheel-rail, (b) Case-2, 1/5 scaled test rig, (c) Case-3, 1/7 scaled test rig

A. Solution Method and Loading Condition

As shown in Fig. 5, the wheel is originally located at position A and set to roll along the rail towards the zone where

the solution is sought. L1 in this figure is the distance, which is needed for the rolling contact to reach the required steady state, while L2 is the distance of solution zone. L1 and L2 are correspondingly 150mm and 30mm for the actual wheel–rail case (Case-1). These dimensions are linearly scaled for the two scaled–cases (Case-2, 3). The origin O is located at the centre of the solution zone, in the middle point of the rail profile. During the rolling of the wheel, a solution is sought at the instant when the centre of the contact patch is at O. All of the mechanical/ geometrical parameters are applied based on the values in Tables II, III. Linear elastic properties are considered in this paper for wheel–rail material. The average rolling speed of 60 km/h is considered for all scenarios.

A combination of vertical and tangential loading is considered in the simulations. The vertical sprung mass on wheel component is assumed 12000, 480 and 245 kg for the cases 1, 2 and 3 correspondingly. The dead weights of the wheel–rail components are automatically included in the numerical analysis. The traction coefficient of 0.15 is applied as the ratio of tangential load to the normal pressure in all cases. Note that the contact surfaces of both the wheel and the rail are smooth. Frictional rolling contact problem is treated in all cases by applying a constant friction coefficient between the wheel and the rail material.

IV. Results of FE Simulations

The normal and tangential problem of wheel–rail contact has been solved for different FE models. Fig. 7 gives the 3D distributions of contact pressure for different models.

The results of adhesion–slip area distributions in the contact patches are demonstrated in Fig. 8, for different FE models. Every block or bullet in the plots represents a node in the FE model. As can be seen for each model, the adhesion area is located at the leading part of the contact patch and decreases in size with the increase in the tangential load.

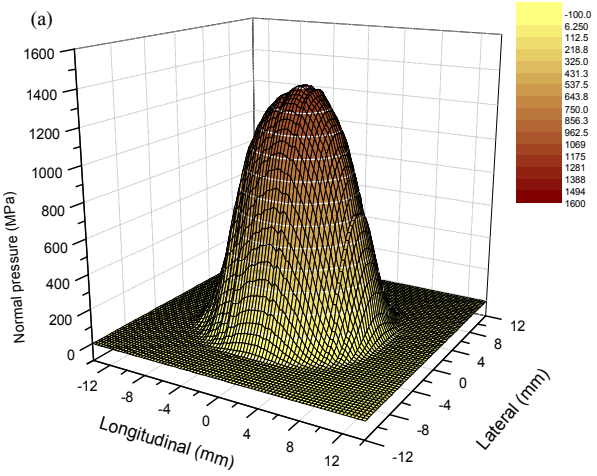

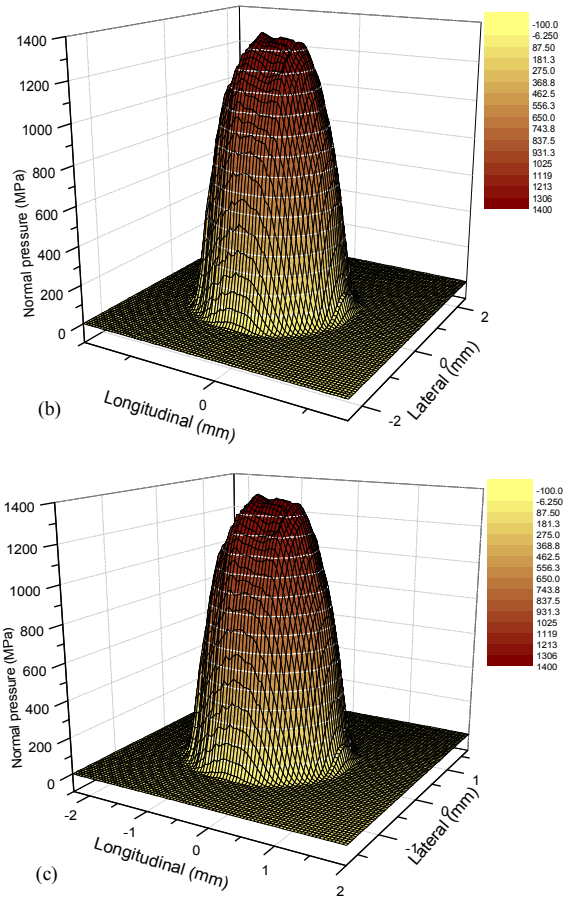

Fig. 7 Distributions of contact pressure for (a) Case-1, actual wheel-rail, (b) Case-2, 1/5 scaled test rig, (c) Case-3, 1/7 scaled test rig

The results of FE simulations for the prescribed models (3 cases) are summarized in Table IV. This table compares the outputs of contact patch areas and dimensions in different models together with their maximum stress responses. As can be expected, the size of contact patch is significantly reduced with the application of geometric scaling. The scaling rate of diagonals in the elliptical contact patches is in good agreement with the linear scaling of dimensions that is proposed in dimensional analysis (see Tables II, III). It is furthermore interesting to see the reduction rate of the contact areas, approximately with the second order of scale factors, as it is anticipated earlier in Table I.

TABLE IV
Summary of Results for FE Simulations

Parameter	Unit	Case–1	Case–2	Case–3
Vertical Load	N	120000	4800	2449
Semi–radius	a (mm)	6.03	1.21	0.86
	b (mm)	8	1.6	1.14
Area	mm^2	151.53	6.07	3.09
Max. Pressure	MPa	1343	1333	1326
Max. shear stress	MPa	447	444	441
Max. V–M stress	MPa	940	933	928

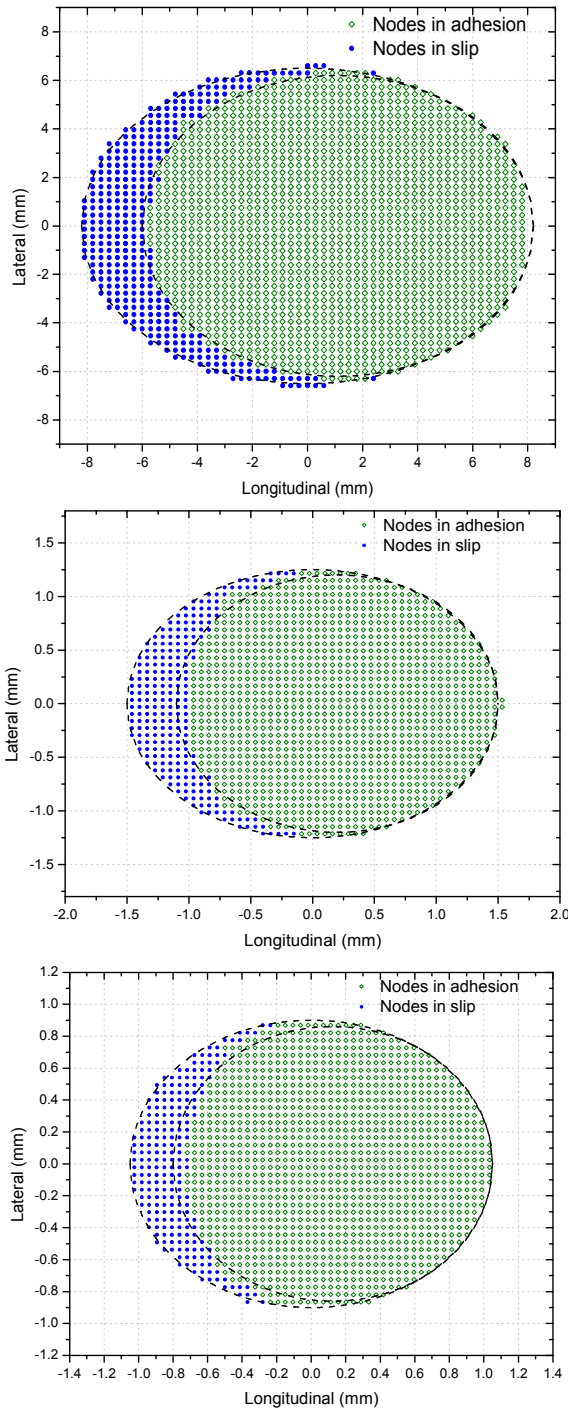

Fig. 8 Distributions of adhesion–slip zones of contact patch for (a) Case-1, actual wheel-rail, (b) Case-2, 1/5 scaled test rig, (c) Case-3, 1/7 scaled test rig

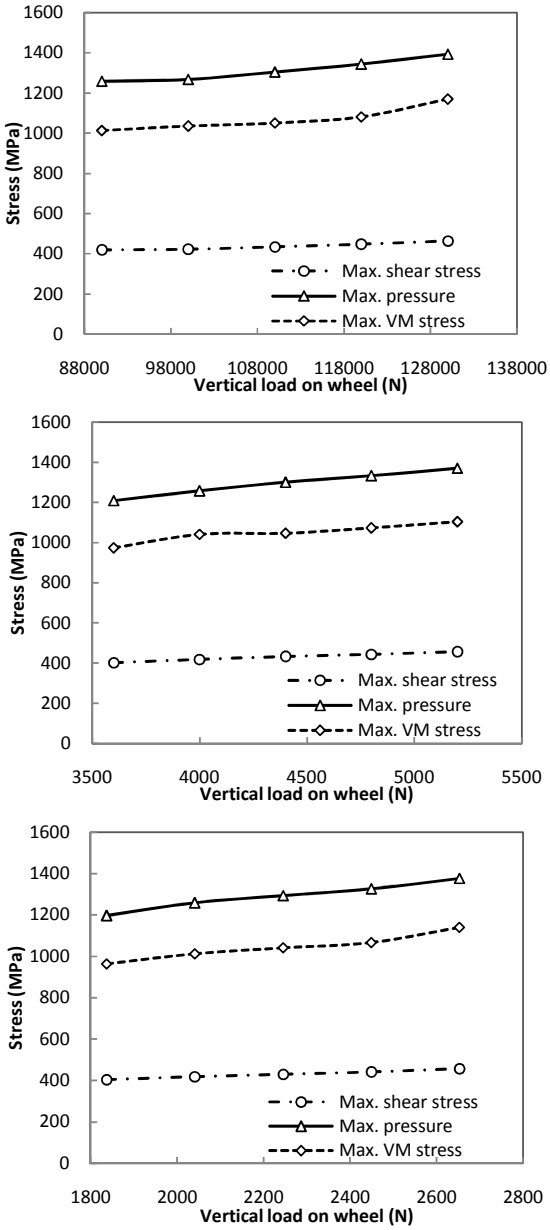

Fig. 9 The results of stress responses in different cases by changing the load levels for (a) Case-1, actual wheel-rail, (b) Case-2, 1/5 scaled test rig, (c) Case-3, 1/7 scaled test rig

V. Discussion

Looking at Table IV, some effects of the scalling on the results of mechanical simulations are transparent. In contrast to the contact patch size, the stress response of FE models has almost a constant range of variation, when the scale factor is changed from an actual system to the 1/5 and 1/7 cases irrespective to the scale factors. It is worth noticing that the stress levels of the scaled cases remained almost in the vicinity of stresses in the real size model. This means that, in spite of having far lower contact areas, the reduced scale cases can generate the same level of contact stresses. It is noteworthy

that the vertical and tangential loads of the scaled cases have been assumed to reduce with the scale factors of $1/N^2$ in each case. Applying such scaled loading conditions on the models, have caused the stress responses to remain unvaried. This finding is a leading indication about the amount of loads that needs to be applied on a scaled test rig to generate the same level of stress in materials. The table gives estimation about the vertical load in two scaled cases, while they have created approximately near stress responses. Taken together, these results suggest that the decreasing rate of the load values for the scaled cases follows almost a sharp reduction with the second power of the scale factor ($1/N^2$). This finding further, confirms the particular associations between different parameters of the reduced scale configurations, proposed in Table I.

In addition to the previous discussion, it is also encouraging to see the effect of different loading conditions in various FE models. A sensitivity analysis is therefore carried out by employing different load levels on the previous numerical models. Five different values of vertical load are applied on each model and the results of maximum stresses are derived as demonstrated in Fig. 9. The same values of traction coefficient are applied for all cases (0.15). As can be seen in Fig. 9, irrespective to the scale factor, the contact stresses from the FE analysis are gradually dropped by declining the vertical wheel load on the rail. Fig. 9 depicts the results of maximal vertical, shear and Von–Mises stresses for different wheel loads. According to these results, the reduction rate of stresses is negligible, since a slight change in load levels is considered.

VI. Conclusion

A new small–scale test rig was developed to study rolling contact fatigue in wheel–rail material. The article dealt with the dimensional analysis, scaling strategy and mechanical design of the prescribed test rig. As a general scaling strategy of the new test rig, dimensions of the wheel–rail elements in the test facility intended to be minimized in order to reduce the construction costs and operational difficulties. However, as the emphasis was laid on the realistic representation of the wheel–rail contact stresses of materials relative to the real operational condition, the scale factor was finalized based on the results of mechanical simulations. Finite element modelling employed for the design process of the new test rig. Different FE models were thus developed for wheel–rail rolling contact problem. An upper and a lower scale (1/5 and 1/7) were defined to perform numerical simulations. Applying the prescribed values of overall scales, the results of dimensional analysis for the equivalent one–fifth and one–seventh scaled rigs were determined and all the scale factors extracted for different parameters of the models. Solution of wheel–rail contact in frictional rolling condition presented for the actual case and two scaled models. Based on the obtained results of FE simulations, the following conclusions can be drawn:

1. A strong evidence of approximate stress levels in different scaled models were observed, while the differences between contact area size and dimensions of various models were huge.
2. The results of mechanical simulations suggest that, if the loading condition is elaborately tuned up with the appropriate ranges, the material's stress in test rig models can reach to that of actual railway. Indeed, it can be concluded that, by applying an overall scale of 1/5 or 1/7 together with the appropriate scaling on loading conditions, it is possible to reach the same contact stresses of actual (full-scale) system.
3. Numerical investigations confirmed the effectiveness of dimensional analysis in the test rig with respect to various input and output parameters. Variations of resulting stresses, strains and contact areas were well in accordance with the predicted scale factors of the dimensional analysis.
4. Although the 1/7 scale configuration benefits from a cheaper, easier and more manageable strategy compare to the 1/5, it is eventually decided to make the new test rig with the overall scale of 1/5 (as the basic scale) and provide the flexibility of having smaller wheel–track elements according to the 1/7 scale. This is mostly because, for 1/7 scale case, a very small contact patch size between wheel and rail was obtained, which is not desirable for emersion of RCF defects on rail.
5. The presented results reveal that the new test rig is able to keep the mechanical properties of the system in similarity with the actual condition, and can generate wheel–rail contact stresses with satisfactory range. These can be achieved by applying the proposed scale factors on different parameters.

The proposed test rig, which is capable of subjecting rail material to a semi–actual contact stress conditions, provides worthy insights leading to optimization of materials in the tribological wheel –rail contact system.

Acknowledgment

Construction of a new test rig is part of the research project namely as Development of High–Performance Rail through Intelligent Metallurgy and Engineering (PRIME), in Delft University of Technology. The present investigation is part of that project, which is financially supported by Dutch rail infra ProRail. Their support and cooperation is gratefully acknowledged.

References

[1] C. Esveld, "Modern railway track", Second ed., *MTR-Productions*, Zaltbommel, The Netherlands 2001.
[2] U. Zerbst, R. Lundén, K.O. Edel, R.A. Smith, "Introduction to the damage tolerance behaviour of railway rails – a review", *Engineering Fracture Mechanics*, vol. 76 (2009) pp. 2563-2601.
[3] J.J. Kalker, "Wheel Rail Rolling Contact Theory", *Wear*, vol. 144 (1991) pp. 243-261.
[4] S. Bogdanski, M. Olzak, J. Stupnicki, "Numerical stress analysis of rail rolling contact fatigue cracks", *Wear*, vol. 191 (1996) pp. 14-24.
[5] S. Bogdanski, M. Olzak, J. Stupnicki, "Influence of liquid interaction on propagation of rail rolling contact fatigue cracks", in: *Proceedings from the Second Mini Conference on Contact Mechanics and Wear of Rail/Wheel Systems*, Budapest, Hungary, 1996, pp. 134-143.
[6] S. Grassie, J. Kalousek, "Rolling contact fatigue of rails: characteristics, causes and treatments", in: *Proceedings of 6th International Heavy Haul Conference*, The International Heavy Haul Association, Cape Town, South Africa, 1997, pp. 381-404.

[7] J. Seo, S. Kwon, H. Jun, D. Lee, "Numerical stress analysis and rolling contact fatigue of White Etching Layer on rail steel", *International Journal of Fatigue*, vol. 33 (2011) pp. 203-211.
[8] Z.F. Wen, L. Wu, W. Li, X.S. Jin, M.H. Zhu, "Three-dimensional elastic-plastic stress analysis of wheel-rail rolling contact", *Wear*, vol. 271 (2011) pp. 426-436.
[9] M.R. Aalami, A. Anari, T. Shafighfard, S. Talatahari, "A robust finite element analysis of the rail-wheel rolling contact", *Adv Mech Eng*, (2013).
[10] X. Zhao, Z.L. Li, R. Dollevoet, "The vertical and the longitudinal dynamic responses of the vehicle-track system to squat-type short wavelength irregularity", *Vehicle System Dynamics*, vol. 51 (2013) pp. 1918-1937.
[11] P. Clayton, "Tribological aspects of wheel-rail contact: a review of recent experimental research", *Wear*, vol. 191 (1996) pp. 170-183.
[12] P. Clayton, D. Danks, "Effect of interlamellar spacing on the wear resistance of eutectoid steels under rolling-sliding conditions", *Wear*, vol. 135 (1990) pp. 369-389.
[13] P. Clayton, D.N. Hill, "Rolling contact fatigue of a rail steel", *Wear*, vol. 117 (1987) pp. 319-334.
[14] P. Clayton, X. Su, "Surface initiated fatigue of pearlitic and bainitic steels under water lubricated rolling/sliding contact", *Wear*, vol. 200 (1996) pp. 63-73.
[15] V. Dikshit, P. Clayton, D. Christensen, "Investigation of rolling contact fatigue in a head-hardened rail", *Wear*, vol. 144 (1991) pp. 89-102.
[16] P. Allen, "Chapter 15, Scale Testing, in Handbook of railway vehicle dynamics", in: S. Iwnicki (Ed.), *CRC Press*, Boca Raton FL (USA), 2006.
[17] C. Heliot, "Small-scale test method for railway dynamics", *Vehicle System Dynamics*, vol. 15 (1986) pp. 197-207.
[18] A. Jaschinski, H. Chollet, S. Iwnicki, A. Wickens, J. Würzen, "The application of roller rigs to railway vehicle dynamics", *Vehicle System Dynamics*, vol. 31 (1999) pp. 345-392.
[19] B.G. Eom, B.B. Kang, H.S. Lee, "Design of small-scaled derailment simulator for investigating bogie dynamics", *International Journal of Railway*, vol. 4 (2011) pp. 50-55.
[20] M. Gretzschel, A. Jaschinski, "Design of an active wheelset on a scaled roller rig", *Vehicle System Dynamics*, 41 (2004) pp. 365-381.
[21] A. Jaschinski, F. Grupp, H. Netter, "Parameter identification and experimental investigations of unconventional railway wheelset designs on a scaled roller rig", *Vehicle System Dynamics*, vol. 25 (1996) pp. 293-316.
[22] T. Armstrong, D. Thompson, "Use of a reduced scale model for the study of wheel/rail interaction", in *Proceedings of the Institution of Mechanical Engineers, Part F: Journal of Rail and Rapid Transit*, vol. 220 (2006) pp. 235-246.
[23] J. Koch, N. Vincent, H. Chollet, O. Chiello, "Curve squeal of urban rolling stock—Part 2: Parametric study on a 1/4 scale test rig", *J Sound Vib*, vol. 293 (2006) pp. 701-709.
[24] D.J. Thompson, A.D. Monk-Steel, C.J.C. Jones, P.D. Allen, S.S. Hsu, S.D. Iwnicki, "Railway noise: curve squeal, roughness growth, friction and wear", *Real Research UK*, Report: RRUK A, 3 (2003).
[25] X. Zhao, Z. Li, "The solution of frictional wheel–rail rolling contact with a 3D transient finite element model: Validation and error analysis", *Wear*, vol. 271 (2011) pp. 444-452.